ACS APPLIED MATERIALS & INTERFACES

www.acsami.org

Research Article

Immuno-affinity Potent Strip with Pre-Embedded Intermixed PEDOT:PSS Conductive Polymers and Graphene Nanosheets for Bio-Ready Electrochemical Biosensing of Central Nervous System Injury Biomarkers

Razieh Salahandish, Fatemeh Haghayegh, Sultan Khetani, Mohsen Hassani, and Amir Sanati Nezhad*

Cite This: *ACS Appl. Mater. Interfaces* 2022, 14, 28651−28662

Read Online

ACCESS | Metrics & More | Article Recommendations | Supporting Information

ABSTRACT: Future point-of-care (PoC) and wearable electrochemical biosensors explore new technology solutions to eliminate the need for multistep electrode modification and functionalization, overcome the limited reproducibility, and automate the sensing steps. In this work, a new screen-printed immuno-biosensor strip is engineered and characterized using a hybrid graphene nanosheet intermixed with the conductive poly(3,4-ethylenedioxythiophene) polystyrene sulfonate (PEDOT:PSS) polymers, all embedded within the base carbon matrix (GiPEC) of the screen-printing ink. This intermixed nanocomposite ink is chemically designed for self-containing the "carboxyl" functional groups as the most specific chemical moiety for protein immobilization on the electrodes. The GiPEC ink enables capturing the target antibodies on the electrode without any need for extra surface preparation. As a proof of concept, the performance of the non-functionalized ready-to-immobilize strips was assessed for the detection of glial fibrillary acidic protein (GFAP) as a known central nervous system injury blood biomarker. This immuno-biosensor exhibits the limit of detection of 281.7 fg mL^{-1} (3 signal-to-noise ratio) and the sensitivity of 322.6 Ω mL pg^{-1} mm^{-2} within the clinically relevant linear detection range from 1 pg mL^{-1} to 10 ng mL^{-1}. To showcase its potential PoC application, the bio-ready strip is embedded inside a capillary microfluidic device and automates electrochemical quantification of GFAP spiked in phosphate-buffered saline and the human serum. This new electrochemical biosensing platform can be further adapted for the detection of various protein biomarkers with the application in realizing on-chip immunoassays.

KEYWORDS: *conductive ink composite, bio-ready electrode, electrochemical biosensing, autonomous microfluidics, point-of-care, central nervous system injury*

1. INTRODUCTION

An ever-growing trend of developing point-of-care (PoC) and wearable electrochemical biosensing platforms is a rational response to the increasing demand for early-stage disease diagnosis, prognosis, and monitoring.[1,2] However, conventionally fabricated biosensors are constrained due to the limited fabrication reproducibility and commercial scalability, thereby limiting their translation into clinically applicable tools.[3,4] The number of steps involved in the preparation and functionalization of electrodes directly contribute to the reproducibility of biosensors. Decreasing the number of biosensor's preparation steps (e.g., synthesizing multiple layers of nanomaterials and deposition of cross-linkers needed for adding functional groups) would be crucial to elevate the overall reproducibility and scalability of these biosensing platforms.[5]

To create electrochemical biosensors with the capability of detecting protein analytes with <1 pg/mL concentrations, conductive nanomaterials have been added to or deposited on electrodes.[6] These nanomaterials increase the conductivity and surface area of the electrodes and provide increased binding sites for cross-linkers. The surface enhancement is then followed by adding specific functional groups, for example, amine or carboxyl moieties, which are prone to form covalent bondings to the immobilizing capture molecules (e.g., antibodies,[7] aptamers,[8] enzyme layers and selective membranes,[9] and molecularly imprinted polymers[10]). Conductive nanomaterials, such as nanosheets of reduced graphene oxide[11] or polyaniline-like polymers,[12] have been employed for surface modification of electrodes. These multilayer coatings have improved the detection sensitivity of electrochemical bio-

Received: April 25, 2022
Accepted: June 3, 2022
Published: June 15, 2022

https://doi.org/10.1021/acsami.2c07322
ACS Appl. Mater. Interfaces 2022, 14, 28651−28662

Scheme 1. Schematic Representation of the Embedded Nanomaterial Structures and the Fabrication Process for the Graphene Intermixed Poly(3,4-ethylenedioxythiophene) Polystyrene Sulfonate (PEDOT:PSS) Carbon (GiPEC) Bio-Ready Strip[a]

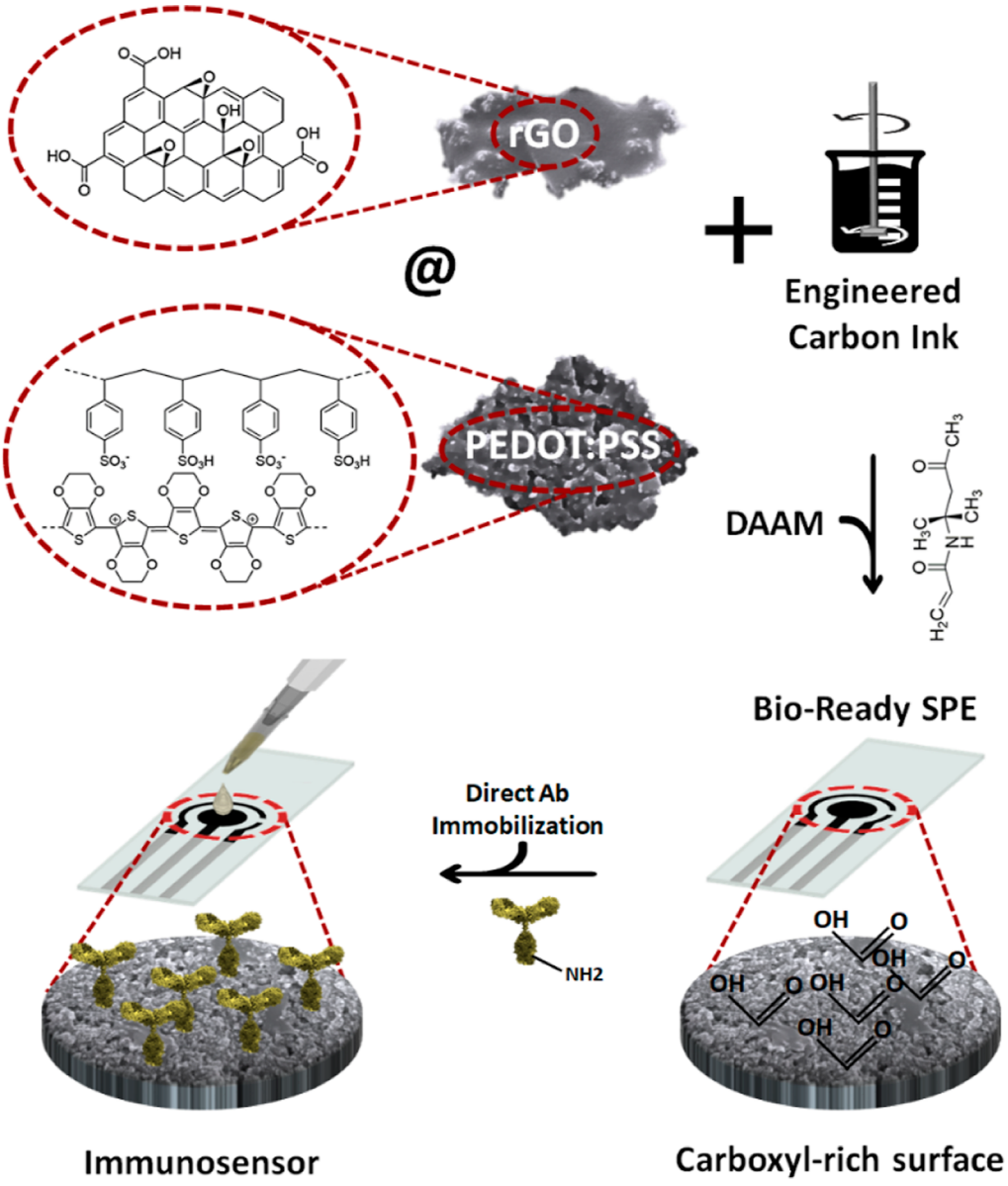

[a]Graphene nanosheets containing the required carboxyl functional groups as well as PEDOT:PSS conductive polymers were mixed in an engineered carbon ink using programmed mechanical stirring with added DAAM binder for increased ink uniformity and consolidation. The resulting bio-ready electrode surface contains the carboxyl functional groups, equipping the surface with immuno-affinity properties, useful for reproducible single-step antibody immobilization for the preparation of the desired immunosensor.

sensors by 2−3 orders of magnitude higher than enzyme-linked immunosorbent assays.[12−15]

New deposition techniques have been attempted to tackle the challenges associated with the complex and multistep deposition of nanomaterials on electrodes needed for scalable and reproducible production of biosensors.[16] Moreover, new fabrication and deposition platforms, such as on-chip electrodepositing of conductive nanomaterials within microfluidics (NanoChip)[3] and on-chip deposition of microfibers,[17] microcarriers,[18] and integrated nanostructures[19] have offered reproducible deposition of different nanocomposites on electrodes. These techniques are only appropriate for laboratory-scale fabrication, and in case of clinical demands, they deliver expensive mass manufacturing and limited throughput due to the need for several electrodeposition steps and time-consuming rinsing and drying phases.

The second step of biosensor preparation is the addition of functional groups, either amine or carboxyl moieties, on the nanomaterial-coated electrode to further immobilize capture molecules.[20] This process adds one or more sub-steps to the sensor preparation process and often requires lengthy incubations. This manual process obviously affects the reproducibility of biosensors.[21] Finally, the antifouling characteristics of an affinity-based biosensor is a crucial consideration in biosensor preparation.[22] For example, a composition of cross-linked bovine serum albumin (BSA) containing a network of reduced graphene oxide nanoparticles on gold-coated glass was deposited to introduce antifouling

https://doi.org/10.1021/acsami.2c07322
ACS Appl. Mater. Interfaces 2022, 14, 28651−28662

properties to electrodes.[23] Novel electrode material inks need to inherently express antifouling properties and self-contain conductive nanostructures and functional groups in order to minimize intermediate surface modifications and add to the reproducibility of the sensors. Ideally, the needed conductivity and functionality of the electrode can be added to the inks during its printing.

Efforts have been made to functionalize graphene on carbon screen-printed electrodes (SPEs).[24] This process, though, has been a challenge owing to the complexity of the production process and ubiquity of the material, equipment, and processing time. Some challenges have been addressed using a one-step nanomaterial coating using polynorepinephrine or polycatecholamine for adding amine functional groups to the surface,[25] or two-step nanoparticle doping,[26] increasing the surface area and conductivity of SPEs as well as functionalizing the electrode surface. For example, polycatecholamine with a rich source of carboxylate or amine[27] was used for a single-step fabrication of ultrasensitive immuno-biosensors.[25] While they showed their high reproducibility in their clinical performance, the uniform coating of these nanomaterials on SPEs using drop-casting, contact printing, or electrochemical deposition methods is subject to the risk of the coffee-ring effect or weak anchoring to the substrate.[24,28]

Engineering the chemistry of the printing ink, mainly by the addition of conductive fillers, has been used to manipulate the surface or tune the mechanical properties of the printed electronics to showcase the desired characteristics.[29] For example, metal nanoparticles and nanowires, such as silver copper or gold, were added to the solvent needed for the preparation of printable ink.[30,31] However, challenges exist in printability of their high material loading, such as possible fractures in the printed constructs and particle agglomeration. Another approach for creating the desired conductivity in these inks is the addition of carbon nanostructures, such as graphene[32] or carbon nanotubes.[33] To eliminate constraints related to complications of nanoparticle mixing, conductive polymers, such as poly(3,4-ethylenedioxythiophene) polystyrene sulfonate (PEDOT:PSS), polyanilines (PANI), and polypyrrole (PPy), have been used in the preparation of conductive printable inks.[34,35] The addition of these materials to printing inks has been primarily explored in wearable strain, pressure, and temperature sensors in stretchable patch formats.[36,37] Their combination with the printing ink can be further used for developing self-contained functional electrodes for electrochemical biosensing.

To this end, graphene existing in the form of graphene oxide (GO) or reduced graphene oxide (rGO) has been extensively used as an added nanomaterial to promote sensor stability while also providing carboxylic functional groups.[11] On the other hand, the use of conductive polymers was shown to be favorable over metal or metal oxide nanoparticles, given their compatibility with uniform printing and cohesion of the ink.[38] Among all conductive polymers, the compatibility of PEDOT:PSS with graphene in sensing applications has been previously explored.[39] The fabrication steps of making biosensors using these materials still contain time-consuming electrodeposition or inkjet printing of the coating materials[40] and lengthy surface activation and functionalization.[39,41] These fabrication methods are suitable for laboratory-scale sensor development, but they lack the characteristics needed for scalable biosensor production.

This work presents a new Graphene@poly(3,4-ethylenedioxythiophene) polystyrene sulfonate (PEDOT:PSS) hybrid ink embedded into the carbon ink and an optimized fabrication process to reproducibly print them on a flexible substrate (Scheme 1). Along with increasing the electrode's surface area, it directly provides the needed functional moieties, which abundantly exist in the reduced graphene oxide nanosheets (illustrated in the schematic), in a single-step printing on the surface for the detection of molecules without the need for any intermediate step.[42] The electrode's surface chemistry was characterized by investigating its morphology, conductivity, and the existence of the functional groups. Moreover, by coupling this new SPE and capillary-based microfluidic chip, we developed an automated electrochemical sensing approach. This autonomous immuno-biosensor quantified the concentration of glial fibrillary acidic protein (GFAP), the known traumatic brain injury (TBI) biomarker,[43,44] in spiked phosphate-buffered saline (PBS) and the human serum. GFAP in the serum of patients with mild traumatic brain injuries and concussion is elevated to 30−100 pg mL^{-1} concentration as opposed to <1−10 pg mL^{-1} in healthy subjects.[45] This concentration also reaches 1.5−5 ng mL^{-1} for patients with moderate traumatic brain injuries. Clinicians have extensively highlighted the PoC need for detecting brain injury biomarkers like GFAP using highly sensitive PoC diagnostic platforms.[46] The fabricated PoC GFAP immuno-biosensor addresses this unmet technological need and enables detecting GFAP in the human serum.

2. EXPERIMENTAL SECTION

2.1. Fabrication of SPEs. AutoCAD 2021 Version: R.47.0.0 was used to design the electrode patterns. The standard three-electrode configuration, containing a working electrode (WE) with a diameter of 4 mm, a reference electrode, and a counter electrode, was used to make the sensors. The engineered low-viscous PEDOT/PSS/Graphene nanostructure hybrid compound dispersed in dimethylformamide (Sigma, USA) (10% w/w) was mixed with the customized carbon ink to make it compatible with the screen-printing technology. Then, diacetone acrylamide (DAAM) (Fisher Scientific, Canada) as a binder was added to the mixture to contribute to the effective consolidation and increase the ink consistency. The mixing step was optimized to 1 h gradually increasing the mechanical stirring with a rotational speed from 50 to 100 rpm. The electrodes were printed by the Micro Flatbed Printer (A.W.T. World Trade, Inc., USA) and using a polyester mesh with 295 mesh/inch and 48 μm thread diameter. All the working, counter, and reference electrodes were printed using the same intermixed ink on a laminated sheet from two identical poly(ethylene terephthalate) (PET) substrates (ST505, $Melinex_R$) attached together by an adhesive (467MP adhesive transfer tape, 3M, USA) to reach the thickness of 0.012″. The silver ink (5025 Silver Conductor, Dupont, USA) was used to print the connector segments of the electrode design. Following the printing step, the wet electrodes were cured in a temperature-controlled process on an InfraRed curing machine (Customized Natgraph Air Force Dryer, Natgraph Ltd, UK) with the roller speed of 10 ft min^{-1} and temperature units of 110, 120, and 140 °C for the overall duration of 10 min. The temperature-controlled curing process enables the gradual evaporation of the ink-binding solvents and prevents the formation of amorphous rough surfaces and micro-cracks. To warrant consistency in the thickness of the printed ink, a Digimatic indicator (Mitutoyo ID-H0530E, Mitutoyo America Corporation, USA) was used to perform quality control. It measured the thickness of the printed ink at multiple spots on the substrate. The thicknesses of carbon and Graphene@PEDOT:PSS-Carbon (GiPEC)-10% and GiPEC-20% electrodes were measured to be 7 ± 1 and 7 ± 2 μm, respectively.

https://doi.org/10.1021/acsami.2c07322
ACS Appl. Mater. Interfaces 2022, 14, 28651−28662

2.2. Modification of the Electrode's Surface. To examine whether any surface modification is needed for antibody immobilization on GiPEC electrodes, the sensing performance of bare GiPEC electrodes was compared to the GiPEC electrodes treated with 3-aminopropyl)triethoxysilane (APTES) (#440140, Sigma, USA), *N*-hydroxysuccinimide (NHS) (#130672, Sigma, USA), and 1-ethyl-3-(3dimethylaminopropyl)carbodiimide (EDC) (#25952-53-8, TCI AMERICA, USA). For preparing the APTES-treated GiPEC electrodes, the APTES solution of 1% (V/V) dissolved in the deionized (DI) water was prepared and drop-cast on the WE while incubated for 12 h at the room temperature. About half of the APTES-coated GiPEC electrodes were rinsed with the DI water and dried at the room temperature prior to antibody immobilization. A solution containing 80 mM NHS and 60 mM EDC in the DI water was drop-cast on the bare GiPEC electrodes as well as the other half of the APTES-coated electrodes and incubated for 4 h at the room temperature prior to rinsing and antibody immobilization. All electrochemical signals were measured in the presence of a solution containing the redox probe of 2.5 mM potassium ferricyanide (III) (#702587, Sigma, USA) and 2.5 mM potassium hexacyanoferrate (II) trihydrate (#33358, Alfa Aesar, Thermo Fisher Scientific., USA) prepared in 1× PBS.

2.3. Preparation of the GFAP Immuno-Biosensor. The bare GiPEC electrodes were immobilized with 10 μg mL^{-1} GFAP antibody (#G3893, Monoclonal anti-glial fibrillary GFAP antibody, Sigma Aldrich, USA) by drop-casting 5 μL of the aliquoted concentration of the antibody on the WE. For the completion of the interaction of the antibody and the electrode's surface, drop-cast GiPEC electrodes were incubated for 60 min at room temperature, followed by incubation at 4 °C overnight. To maintain the drop-casted antibody solution in the liquid phase and prevent its evaporation, a water-absorbed pad was placed inside the Petri dish containing the electrodes, and the Petri dish was sealed using parafilm. BSA (#sc-2323, ChemCruz, USA) with a concentration of 0.005% (m/v), prepared in 1× PBS, was used as the blocking agent to cover the blank spaces of the antibody-coated electrodes and avoid further non-specific binding. The BSA solution was drop-cast, with a volume of 5 μL, onto the WE, incubated for 20 min at the room temperature, and rinsed and dried before the biosensing step. Various concentrations of GFAP antigen (#345996, GFAP, Human Brain, EMD Millipore Corp., USA) were prepared through a serial dilution of the spiked GFAP protein in PBS (1×, Growcells, CA, USA, pH = 7.4) and the human serum. The optimal incubation period for GFAP antibody−antigen immunoreaction was determined to be 30 min for the incubation at the room temperature for the spiked samples drop-cast on the GFAP biosensor. After the incubation period, the sensors were rinsed three times in the DI water, dried, and then, electrochemical impedance spectroscopy (EIS) measurements were conducted using a PGSTAT 204 Potentiostat/Galvanostat (Metrohm, USA) for obtaining the calibration curve. A solution of 2.5 mM of potassium ferricyanide (III) (#702587, Sigma, USA) and 2.5 mM potassium hexacyanoferrate (II) trihydrate (#33358, Alfa Aesar, Thermo Fisher Scientific., USA), prepared in 1× PBS, was again used as the redox reagent. Human blood samples were collected from healthy individuals (Ethics# #REB15-2138.) in 5 mL Eppendorf tubes and allowed to be clotted at room temperature for 30 min. The clotted samples were then centrifuged for 5 min at 1000 relative centrifugal force. The serum was separated from the blood using BD Vacutainer Plus Serum tubes (BD, Ontario).

2.4. Design and Fabrication of the Capillary Microfluidic Chip. All the layers of the capillary microfluidic chip used in this study were designed using AutoCAD 2021 Version: R.47.0.0. A Speedy 360 flex CO_2 laser engraver machine (Trotec, USA) was used to cut the sheet layers of the microfluidic chip, including poly(methyl methacrylate) (PMMA) sheets (Static Dissipative Rigid Plastic sheets, SciCron Tech, USA) of different thicknesses as the fluid layers, pressure-sensitive adhesive (PSA) layers (ARcare 90106NB, Adhesive Research Inc., USA) as either the bonding or fluid layers, and virgin wood fiber tissue wipers (Kimberly-Clark Worldwide, Inc). Finally, nitrocellulose (NC) fibers (PALL Corp., USA) were soaked in 70 mM $[Fe(CN)_6]^{3-/4-}$, dried at room temperature, and assembled within a designated area within the fluid channels prior to sealing the microfluidic chip. The antibody-immobilized and BSA-blocked electrodes were easily inserted into the microfluidic chip for creating a ready-to-use biosensing testing strip. For measuring the electrochemical signals associated with the fabricated immuno-biosensor within the strip, 430 μL of PBS or serum samples containing defined concentrations of GFAP proteins were introduced into the inlet well. Following the delivery of the redox solution automatically to the sensing area after 30 min, the EIS measurements were conducted to obtain charge transfer signals and used to plot the corresponding calibration curves for both the PBS-spiked and serum-spiked samples.

2.5. Surface Characterizations of SPEs. Atomic force microscopy (AFM) in the tapping mode (AFM, Bruker Nanoscope, Germany) and scanning electron microscopy (SEM, JSM-7001FA) were utilized to characterize the topography and morphology of the carbon-based electrodes. Confocal Raman microscopy, Alpha 300 R-WiTec (laser at 532 nm wavenumbers; 60 s accumulation time) was used to obtain the Raman spectra of the electrodes. The attenuated total reflectance/Fourier-transform infrared (ATR/FTIR) spectra of the electrode surface were recorded by ATR/FTIR spectroscopy (Bruker IFS 55 Equinox instrument equipped with an MCT cryodetector). The electrical resistivity (sheet resistance) of the printed conductive films was measured by a four-probe station connected to a multimeter (Keysight 34460A). All electrochemical measurements were performed using the PGSTAT 204 Potentiostat/Galvanostat (Metrohm, USA). The EIS measurements were carried out with a signal amplitude of 10 mV and an open circuit potential (E_{ocp}) of 0.17 V. The frequency range for all the measurements was selected to be sweeping from 20 kHz to 1 Hz. The obtained Nyquist plots were used to determine changes in the charge transfer resistance signals which attribute to the bioanalyte conjugation on the surface. The cyclic voltammetry (CV) signals used for reproducibility tests were conducted through a potential range from −0.8 to 1 V and a scan rate of 100 mV s^{-1}, with all measurements performed in the presence of 2.5 mM redox reagent ($Fe(CN)_6^{3-/4-}$). Contact angle measurements were performed using a Drop Shape Analyzer (DSA 100E, KRUSS Scientific, Germany).

2.6. Pre-Characterization of the Screen-Printed Electrodes. A standard three-electrode configuration, consisting of the working, counter, and reference electrodes, was printed using a uniform mixture of the developed intermixed ink (Figure S1A). The electrode leads were printed with silver ink to minimize the signal loss (Figure S1B). The composition of the printing ink was chemically engineered to express the required conductivity and affinity to biomolecules using the conductive polymers of PEDOT:PSS and the nanosheets of graphene. They were uniformly embedded within a matrix of custom-made carbon ink by employing specific binders and optimizing the mechanical stirring step, resulting in reliable printable ink. Despite its lowermost viscosity among other commercialized screen-printable inks, it could accurately print features down to 300 μm in size in the design of a ready-to-use nine-electrode configuration (Figure S1C). Viscosity is a crucial physical parameter of printable inks which determines the rate and quality of screen printing, minimal achievable feature size, and thickness of the final prints. The engineered conductive material was printed on a flexible PET substrate, considering its potential to be feasibly integrated with the microfluidic chips for PoC or wearable biosensing applications (see details in Section 3.3.1). The PET material is also known to be inert with strong adhesion to the ink but with no interference in its composition. A PSA mask was patterned using a laser cutter and attached to the electrode to electrically isolate the silver leads (Figure S1D). A 3-lead cable was used to connect the printed electrode to a benchtop potentiostat. The electrode design, dimensions, and manufacturing tolerances are provided in Figure S2. The screen printing of the new ink, following the modified method, successfully creates electrodes with 400 μm gaps between each two WEs in a multiplex electrode design (Figure S2C). Such uniform gaps eliminate undesired interconnection of the electrodes possibly occurring due to the leakage of the ink to the neighboring areas during the printing and drying processes. The step-by-step printing process is shown in Figure S3.

https://doi.org/10.1021/acsami.2c07322
ACS Appl. Mater. Interfaces 2022, 14, 28651−28662

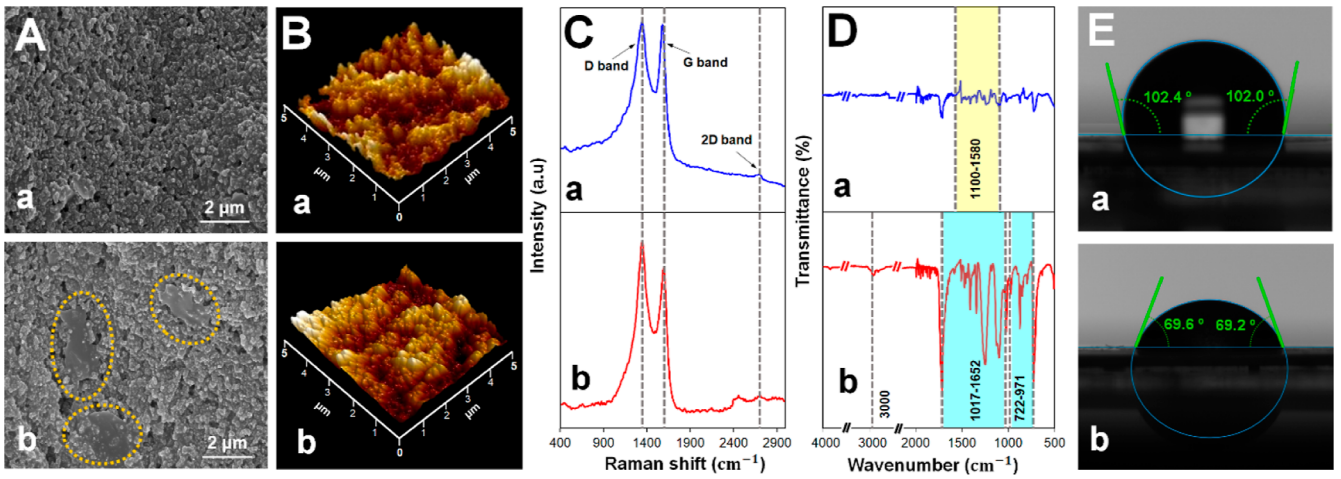

Figure 1. Physical characterization of the GiPEC SPEs. Characterization analysis of both the carbon (a) and GiPEC SPEs (b), including (A) field emission scanning electron micrographs (scale bar: 2 μm), with the highlighted yellow areas vividly depicting the graphene nanosheets, (B) AFM images (5 μm × 5 μm), (C) Raman spectroscopy, (D) ATR, and (E) contact angle measurement at the interface of water and the GiPEC electrode. The measurements were performed in the air as the surrounding phase for (a) carbon and (b) GiPEC SPEs in all characterization methods (A–E).

With a multitude of additives in the carbon-based inks, their effects on the electrical resistivity of the electrodes were characterized. A four-probe station connected to a multimeter positioned on a straight line with 1 mm space between every probe was used to measure the sheet resistance of the conductive material. eq S1 represents the electrical resistivity (R_s) of the sheet measured by the multimeter,[47] where ΔV is the voltage difference between the probes 2 and 3 and I is the electrical current between the outer probes 1 and 4. The electrical conductivity of different inks was characterized using eq S2, where σ is the electrical conductivity and t is the thickness of the printed layer. The electrodes with a nominal thickness of 7 μm were printed uniformly, and their electrical resistivity was measured (Table S1). The electrical conductivities of the carbon, GiPEC-10%, and GiPEC-20% electrodes were measured to be 1624.28 ± 41.29, 1490.31 ± 41.29, and 1032.57 ± 25.06 S m^{-1}, respectively (n = 4; the electrical resistivity was measured at three distinct areas of each electrode). Increasing the weight percentage of the additive hybrid ink (Graphene@PEDOT:PSS) decreased the conductivity of the electrodes. Also, increasing the Graphene@PEDOT:PSS additive ink into the base carbon ink decreased the consistency of the electrodes owing to the decreased viscosity and less printability of the hybrid ink.

3. RESULTS AND DISCUSSION

3.1. Physical Characterization of the Printed Electrodes. The surface morphology of the carbon and GiPEC electrodes was characterized by field emission scanning electron microscopy (FESEM) (Figure 1A(a,b)). The FESEM images of the bare carbon electrode show the distinct presence of the ink binders and a rough surface which itself is suitable for biosensing due to the increased surface area. The presence of the graphene nanosheets is observable [highlighted in yellow circles in Figure 1A(b)] within a uniform surface construct after modifying the carbon ink with the engineered chemistry of the graphene and the conductive polymers. Upon the ink modification, the FESEM visualizations still illustrate the desired morphology, with surface fragments and asperities contributing to further bioanalyte deposition steps. This is evidenced in Figure S4, which shows the surface of GiPEC following the direct antibody immobilization. The image clearly shows that the surface pores specifically the pores of the graphene nanostructure were uniformly filled with the antibodies, confirming the consistent presence of the carboxyl functional groups on the surface.

AFM tapping mode was used to characterize consistency in surface topography of the carbon and GiPEC. The hybrid Graphene@PEDOT:PSS film consists of 0.2 mg mL^{-1} PEDOT:PSS mixed with 1 mg mL^{-1} electrochemically exfoliated graphene, uniformly distributed in the carbon ink matrix. The average values of root-mean-square (RMS) roughness of the carbon and GiPEC films were measured to be 0.289 and 0.470 μm, respectively [Figure 1B(a,b)]. The depth histograms of the GiPEC and carbon electrodes recorded with AFM showed a high uniformity (Figure S5), and together with the RMS values suggest higher roughness for GiPEC compared to the bare carbon electrodes.

Raman spectroscopy was used to analyze carbon and conductive polymers, characterizing the symmetric bonds, for example, C–C bond (Figure 1C).[48] The major characteristic peaks of the GiPEC film are observed between 1300 and 1700 cm^{-1}.[49] The G band at around 1480–1590 cm^{-1} corresponds to the in-plane vibration (E_{2g} phonon) of the sp^2 bonded carbon structure. The D band at around 1320–1450 cm^{-1} reflects the defects (vacancies, grain boundaries, and amorphous carbon species) and disorders in the graphitic structure.[50] The 2D band is also indicated around 2696 cm^{-1}. GiPEC shows a bigger I_D/I_G ratio compared to the carbon electrode, attributed to broken sp^2 bonds. It indicates that the graphene sheets have a chemical interaction with PEDOT:PSS chains and break the hexagonal carbon rings.

ATR/FTIR spectroscopy measured and compared carbon and Graphene@PEDOT:PSS hybrid film spectra. The characteristic bands in the spectrum at 1504 and 1580 cm^{-1} correspond to C–C and C=C, respectively.[51] The absorption bands at 1341 and 1408 cm^{-1} are attributed to the C–O–C band, while the C–C stretching vibration of the quinoidal thiophene is detectable at 1100 cm^{-1}.[51] The absorption bands at 722, 792, 847, 871, and 971 cm^{-1} are assigned to stretching vibrations of the C–S bond in the thiophene ring (Figure 1D). The sulfonate group of PSSs is detectable at 1017 and 1097 cm^{-1} wavenumbers. The bands at 1652 and 3000 cm^{-1} are related to C=O and O–H, respectively. These bonds verify the existence of desired carboxyl functional groups directly introduced to the surface upon the addition of functionalized Graphene@PEDOT:PSS into the carbon ink. The absorption

https://doi.org/10.1021/acsami.2c07322
ACS Appl. Mater. Interfaces 2022, 14, 28651–28662

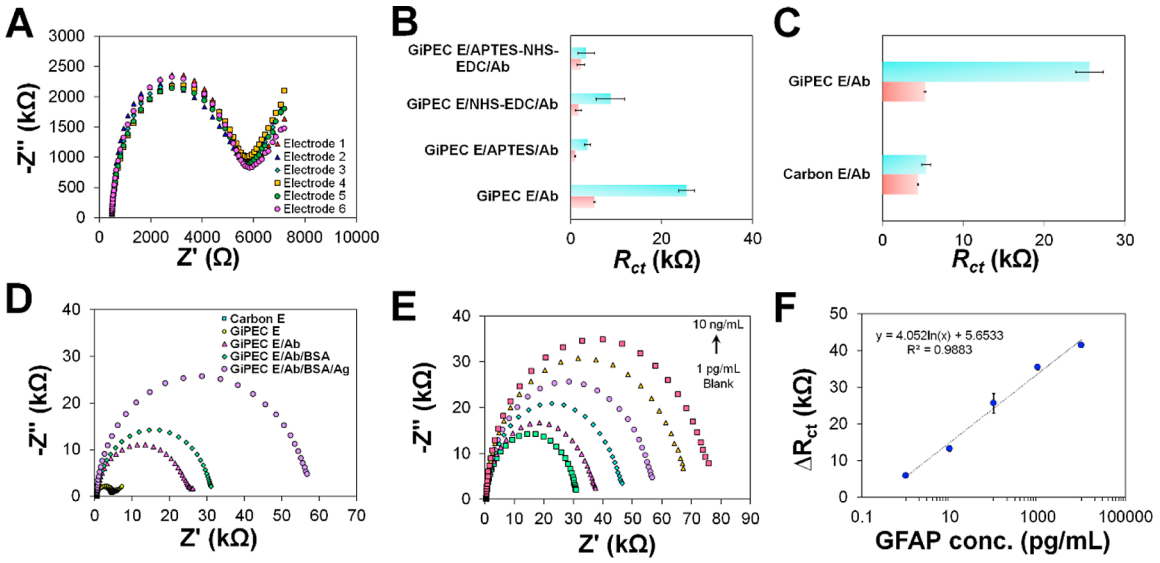

Figure 2. Electrochemical characterization of the carbon and GiPEC SPEs. (A) Electrochemical impedance spectroscopy (EIS) Nyquist plots of the GiPEC electrodes (n = 6) in the presence of 2.5 mM redox solution. (B) Comparison of the functionality of the bare GiPEC and the GiPEC functionalized with APTES, NHS- 1-ethyl-3-carbodiimide hydrochloride (EDC), and APTES−NHS−EDC for antibody (Ab) immobilization. Red bars represent the signal before antibody immobilization and the blue bars depict the after-antibody immobilization signals. (C) Comparison of the Ab affinity immobilized on the GiPEC and carbon electrodes, with blue bars indicating the after-antibody immobilization R_{ct} and red bars indicating the before-antibody immobilization signals. (D) Nyquist plots for the stepwise GiPEC surface modifications, resulting in the creation of the immuno-biosensor. (E) Nyquist plots and (F) corresponding calibration curve of GFAP spiked in PBS. The immuno-biosensor was blocked with BSA and incubated at different concentrations of GFAP. All error bars are stderr (n = 3).

bands of the hybrid film shift toward a higher wavenumber (blue shift by about 1∼3 cm^{-1}) compared to the bands in the pure carbon film.

The contact angle measurement is used to characterize surface wettability in the presence of electroactive solutions. The surface of the GiPEC electrode was subject to contact angle measurement, where it shows a lower contact angle (69.8 ± 0.6)° compared to the carbon electrode (97.1 ± 5.9)° [Figure 1E(a,b)]. This improved wettability is attributed to the abundance of the oxygen functional groups and the lower amount of carbon ink present on the surface of GiPEC electrodes.

The physical characterizations of GiPEC SPEs verify the improved uniformity of the carbon electrode upon the addition of Graphene@PEDOT:PSS hybrid ink. In addition, the ATR graph indicates the presence of the carboxyl functional groups on the surface of the GiPEC electrode. These functional groups would form a covalent amidic binding between the electrode and the bio-capture molecules (e.g., antibodies here). Therefore, the presence of carboxyl groups eliminates the need for any additional cross-linker needed for the immobilization of capture molecules on the electrodes.

3.2. Electrochemical Characterization of GiPEC SPEs and GFAP Biosensors. *3.2.1. GiPEC SPEs versus Other SPEs.* As a novel SPE with a variety of potential applications in immunosensing of different proteins, the electrochemical properties of the GiPEC and the unmodified carbon SPEs were characterized using EIS and CV electrochemical techniques. Additionally, the electrochemical properties of DS-110 and DS-150 carbon SPEs (manufactured by Metrohm, DropSense) of identical electrode designs were measured and used to compare the performance of electrodes. The EIS measurements reveal the formation of the complete semi-circle in Nyquist plots (Figure 2A), representing the creation of the corresponding real and imaginary impedances and capacitance on the electrodes. The reproducibility of the printed carbon and GiPEC electrodes (selected from different batches printed at different time points and stored in the laboratory environment for over 6 months) was determined by measuring CV and EIS signals in the presence of 2.5 mM $Fe(CN)_6^{3-/4-}$ redox probe (n = 6) (Figure S6A−D). The relative standard deviation (RSD) of the charge transfer resistance (R_{ct}) obtained from Nyquist plots is calculated to be 4.07% for the GiPEC electrode and 3.13% for the carbon electrode, which verifies their highly reproducible printing compared to RSD of 29.06 and 29.92% for the DS-110 and DS-150 commercial DropSens carbon electrodes, respectively (Figure S7). This comparison indicates that the Graphene@PEDOT:PSS ink is uniformly mixed with the carbon base ink, wherein the curing process performed in a programmed temperature cycle did not alter the structure of the functional groups. Figure S8 compares R_{ct} for four different types of electrodes tested in this work. The results confirm a much higher reproducibility of the carbon and GiPEC electrodes.

The electrochemical reaction mechanism of the redox probes on the surface of the GiPEC electrodes was evaluated using the CV test with the scan rate ranging from 10 to 700 mV s^{-1} (Figure S9A). The reduction and oxidation peak currents were plotted as a linear relationship between the peak current and the square root of the scan rate (Figure S9B,C), affirming the diffusion control process of the redox species on the electrode.

To verify that the fabricated GiPEC electrodes are functional in terms of direct conjugation with antibodies without any need for cross-linkers, the performance of several cross-linking candidates on the GiPEC electrode was examined and compared to the no-cross-linker condition. In a previous study, the hydroxyl functional groups in Graphene@PEDOT:PSS were modified with APTES and Succinic Anhydride (SA) for successful binding of aptamers to

https://doi.org/10.1021/acsami.2c07322
ACS Appl. Mater. Interfaces 2022, 14, 28651−28662

Table 1. Comparison of Research Works on Developing Immuno-Biosensors with Minimum Number of Functionalization Steps[57,25,58−65]

Base Electrode	Electrode's Surface Modification Method	Cross-linker or Activation	Number of surface Modification steps	Modification time	Biomarker	Electrochemical technique	Dynamic range	LOD	Reference
Au SPE	Cysteamine Self-Assembled Monolayer formation	(NHS-EDC)	two	> 8 hrs	S100B (TBI biomarker)	EIS	10–1000 pg mL^{-1}	18 pg mL^{-1}	57
Graphene SPE	Polycatecholamines nanofilm electropolymerization	None	one	-	Ubiquitin carboxyl-terminal hydrolase (UCHL-1)	SWV	0.1-100,000 pg mL^{-1}	1.91 pg mL^{-1}	25
Polyimide film	Graphene Laser-Induction	Carbodiimide crosslinking (NHS/EDC)	two	> 1 hr	Salmonella enterica serovar Typhimurium	EIS	25-100,000 CFU mL^{-1}	13.7 CFU mL^{-1}	58
Glassy Carbon Electrode (GCE)	Epoxy Functionalized Polymer(EFP) – carbon nanotube composite	None	one	> 5 hrs	IgG	DPV	0.1 - 25 ng mL^{-1}	0.05 ng mL^{-1}	59
Bare Gold	Polyethyleneimine (PEI)	Carboxylated CNTs (COOH–CNT) – (NHS-EDC)	two	< 2 hrs	Cardiac Troponin T (cTnT)	Amperometry	0.1-10 ng mL^{-1}	0.033 ng mL^{-1}	60
Graphene decorated interdigitated electrode	2-Aminobenzyl amine (2-ABA) Electrofunctionalization	None	one	-	Cardiac Troponin I (cTnI)	LSV - EIS	0.01 – 1 ng mL^{-1}	0.01 ng mL^{-1}	61
Carbon SPE	Graphitic carbon nitride (g-C_3N_4) – coated with Fe_3O_4 nanoparticles	None	one	> 1 hr	Tumour marker Carbohydrate antigen 125 (CA125)	Electrochemiluminescence (ECL)	0.001– 5 U mL^{-1}	0.4 mU mL^{-1}	62
Gold electrode	Sandwich-based nanogold functionalized graphene	None	one	12 hrs	α-fetoprotein (AFP)	CV	0.1–200 ng mL^{-1}	0.05 ng mL^{-1}	63
Carbon SPE	4- carboxyphenyl diazonium salt electrografting	(NHS/EDC)	two	>1 hr	Survival motor neuron (SMN) protein	voltammetric	1- 100,000 pg mL^{-1}	0.75 pg mL^{-1}	64
Glassy Carbon Electrode (GCE)	Dialdehyde Cellulose (DAC)	None	one	> 7 hrs	Human IgG	DPV	0.5 - 45 ng mL^{-1}	0.3 ng mL^{-1}	65
Graphene@PEDOT:PSS intermixed with carbon ink	**None**	**None**	**Zero**	**Zero**	**GFAP**	**EIS**	**1 -10,000 pg mL^{-1}**	**281.7 fg mL^{-1}**	**This Study**

electrodes.[41] In this study, Yen et el. took advantage of the carboxyl functional groups of SA for immediate interaction with the amine groups of the antibody. In another study, oxygen plasma activated the functional groups of the PEDOT:PSS, leading to the formation of APTES monolayers.[52] In addition, glutaraldehyde[53] and NHS/EDC[54] were also used as cross-linkers for antibody immobilization on the PEDOT:PSS. In this work, different combinations of APTES and NHS/EDC were applied on the GiPEC electrodes to compare their ability in antibody immobilization against GiPEC. APTES 1% (v/v) solution in the DI water was drop-cast on the GiPEC WE and incubated for 12 h to form the amine functional groups. To examine the performance of NHS/EDC in improving the affinity of the surface to antibodies, both the bare GiPEC and the APTES-functionalized GiPEC electrodes were incubated for 4 h with 80 mM NHS solution and 60 mM EDC solution in the DI water. Based on the measured EIS signals, the bare GiPEC electrodes showed superior performance in antibody immobilization compared to the other APTES- and NHS/EDC-functionalized GiPEC electrodes (Figure 2B). This response confirms that the printed ink solely can provide the carboxyl functional groups without the need for any intermediate surface modification or functional group activation. Immobilization of the antibodies on carboxyl-rich surfaces without activation of the functional groups has also been reported previously, which also ensures the covalent bonding between the amine groups of the antibody and the carboxylated bio-ready strip's surface.[55,56] The addition of the Graphene@PEDOT:PSS ink to the base carbon ink, along with an optimized protocol of screen printing, provides a combination of high surface area and active functional groups for antibody immobilization as opposed to other functionalization protocols.

For scale manufacturing of biosensors, fewer numbers of sensor preparation steps are highly desired. As the GiPEC electrode inherently contains carboxyl functional groups, it eliminates the preparation period and the need for cross-linking steps. This unique feature was only present for the GiPEC electrode, wherein the carbon SPEs did not show enough capacity for antibody immobilization (Figure 2C). The EIS signal of the bare carbon electrodes not being significantly different shows that the GFAP antibodies were only specifically bonded to the surface of the GiPEC electrode and not to the carbon electrode. It also confirms that the GiPEC electrode does not require any additional functionalization step and is converted to a biosensor by a single-step drop-casting of the antibody on the electrode.

Table 1 summarizes various chemistries employed in the literature for decreasing the fabrication steps of electrochemical biosensors. All studies explored have claimed to have only one, or a maximum of two, surface modification, cross-linking, or functionalization steps, as a key factor in feasible scalable preparation of immunosensors. Only the method presented in this work uses the bare printed electrode for antibody

https://doi.org/10.1021/acsami.2c07322
ACS Appl. Mater. Interfaces 2022, 14, 28651−28662

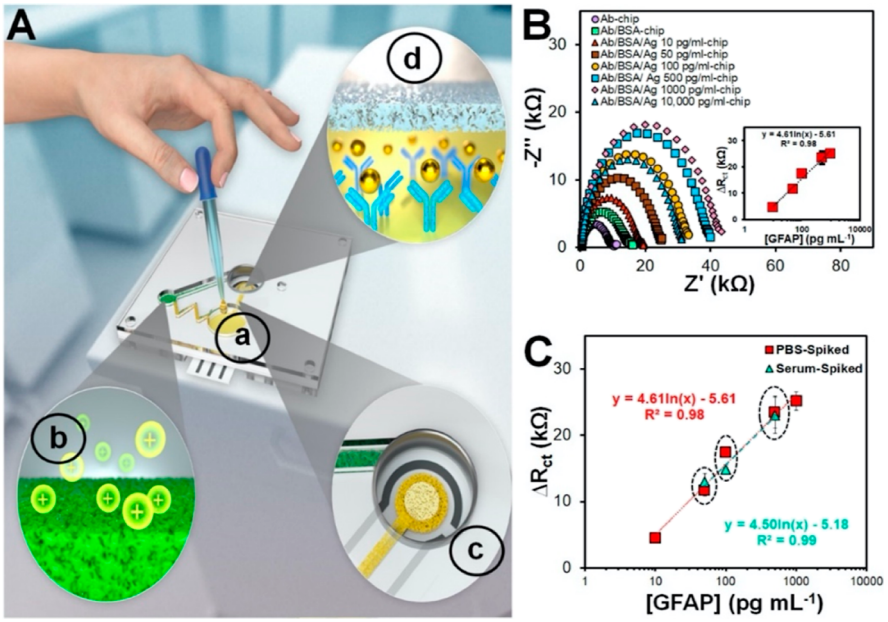

Figure 3. The autonomous microfluidic-integrated GFAP immuno-biosensing assay. (A) Assay representation and its compartments, including (a) inlet reservoir for biosample collection, (b) side redox route where the redox reagents mix with the biosample, and (c,d) biosensing chamber wherein the antibody−antigen interaction occurs on the biosensor. (B) Nyquist plots of the EIS measurements from the electrochemical GFAP immuno-biosensor embedded inside the assay. The inset is the corresponding calibration curve for PoC detection of GFAP samples prepared in PBS. (C) On-chip comparison of serum-spiked and PBS-spiked samples for different GFAP concentrations of 50, 100, and 500 pg mL^{-1}.

immobilization without the need for any other surface enhancement step, which clarifies the concept of zero-step functionalization.

To test the biosensing performance of the GiPECs electrodes, they were examined for the measurement of GFAP concentration. The effect of the serum matrix on the GiPEC and the carbon electrodes was examined and compared to the DS-110 carbon electrodes. First, in the absence of any functionalization or GFAP antibody, the risk of antifouling was assessed on the surface of the bare GiPEC and the carbon SPEs produced in this work. The electrochemical response shows that both the bare carbon and the GiPEC electrodes preserved their electrochemical characteristics verified through the generation of semi-circles in the Nyquist plots in either the human serum or BSA matrices (Figure S10A,B). The variations seen for BSA-deposited samples are attributed to the non-specific binding of this protein to the carboxyl-rich surface, directly deposited before any antibody immobilization (this non-specific binding is minimized during the biosensing step). In these plots, the equivalent circuit $[R_s(R_{ct}Q)]$ was detectable (R_s is the resistance of the solution, R_{ct} is the charge transfer resistance, and Q is the constant phase element). However, for the bare DS-110 carbon electrodes incubated with the human serum, no semi-circle was detectable in the Nyquist plots, confirming the occurrence of biofouling on the DS-110 electrodes (Figure S10C). To warrant that the cast-coating of PBS (a buffer or matrix to spike target biomarkers) on the carbon and the GiPEC SPEs does not alter the signal, the EIS measurements were performed on the electrodes incubated for 30 min with PBS. This test shows that there is no significant difference between the EIS signals of the PBS-mediated GiPEC electrodes and the bare GiPEC electrodes as opposed to the signal generated by BSA and the human serum (Figure S10D).

3.2.2. Electrochemical Characterization of the GiPEC Immuno-Biosensor. The GiPEC electrodes were converted to electrochemical GFAP biosensors by drop-casting the monoclonal GFAP antibody on the electrode, followed by coating 0.005% (m/v) BSA on the electrode to eliminate non-specific binding. The EIS measurement was conducted for the stepwise electrochemical characterization of the GFAP biosensor. The significant increase (330%) in R_{ct} upon immobilizing the GFAP antibody on the bare GiPEC electrode confirms the formation of the insulating antibody layer bonded to the WE (Figure 2D). Electron transfer was hindered by introducing the surface-blocking BSA to the WE, resulting in a 23% increase in the semi-circle radius and a higher charge transfer resistance. The optimized incubation period needed for the interaction between GFAP and its antibody occurred within 30 min (Figure S11A). This incubation period was followed throughout this study. Also, the stability of the immobilized antibodies on the surface of the bio-ready strips, and the EIS signals of antigen-interacted immunosensors, with a concentration of 100 pg/mL, were obtained in a time window of 3−5 h after assay opening in the room temperature, on different days. The associated results, presented in Figure S11B, depict no significant difference between the signals measured at different tested time points, suggesting the stability of the sensor at least within hours of exposing the sensor to the room temperature.

To examine the utility of the immuno-biosensor in detecting GFAP proteins, the EIS signals were measured within the range from 500 fg mL^{-1} to 100 ng mL^{-1}, spiked in 1× PBS, pH = 7.4. This concentration range was selected based on the clinically relevant concentrations of GFAP in the serum of mild TBI patients.[66] The successful quantification of GFAP in PBS was proven when observing a linear increase in R_{ct} in the corresponding calibration curve upon the rise in GFAP antigen concentrations in the samples (Figure 2E,F). The GFAP

https://doi.org/10.1021/acsami.2c07322
ACS Appl. Mater. Interfaces 2022, 14, 28651−28662

immuno-biosensor showed the limit of detection (LoD) of 281.7 fg mL^{-1} [3 signal-to-noise ratio (S/N)], the limit of quantitation (LoQ) of 379.9 fg mL^{-1} (10 S/N), the sensitivity of 322.6 Ω mL pg^{-1} mm^{-2}, and the linear detection range from 1 pg mL^{-1} to 10 ng mL^{-1}, comparable to or better than the other GFAP biosensors developed so far.[45] The RSD values of GFAP immuno-biosensors were less than 10%.

3.3. Automated On-Chip GFAP Biosensing. *3.3.1. Microfluidic-Integrated GFAP Immuno-Biosensing Assays.* To test the functionality of the printed strips in non-conventional automated fluid handling assays, the GiPEC SPEs were integrated into a capillary microfluidic platform, and the concentration of GFAP was measured in spiked PBS samples. In most electrochemical biosensors, biosamples containing the biomarker of interest (e.g., GFAP in this work) are manually deposited on the WE, followed by incubation, washing, and redox probe addition steps prior to recording the electrochemical signal.[67] To automate these steps, a microfluidic assay was developed for true electrochemical PoC biosensing. The biosample delivery onto the WE, incubation within a defined period, washing for removing non-specific binding, and redox probe introduction onto the three-electrode design were automated and followed by the EIS measurement. These steps examine the potential of the embedded electrode in recognizing the proteins of interest without any fouling or non-specific bonding interference. A multilayer microfluidic chip was fabricated where it consists of different compartments (Figure 3A): an inlet biosample reservoir, a side redox route, and a biosensing chamber. PMMA sheets with different thicknesses were cut using a laser cutter to create chamber compartments. PSA was used to bond the fluid layers. Porous tissue wipers made of wood fibers or NC were patterned using a laser cutter and aligned with the fluid layers to control the capillary flow through different compartments and channels. Further explanation with regard to the design of the layer-by-layer microfluidic chip and the role of each layer (Figure S12A) and the stepwise performance of the chip (Figure S12B) is presented in the Supporting Information, section SI VIII.

3.3.2. High-Resolution Electrochemical Detection of GFAP Using PoC Microfluidic-Integrated Immuno-Biosensor. The performance of the GiPEC-based GFAP immuno-biosensor was examined for the detection of GFAP with different concentrations spiked in PBS and human serum inside the microfluidic strip. The EIS measurements of the on-chip GFAP biosensor were used to obtain the signal calibration curve. The optimal biosample volume of 430 μL was needed to run the 30 min biosensing assay developed in this work. Here, the optimal period of antibody and antigen interaction (30 min for GFAP in this work shown in Figure S11) was used to design the operational duration of key compartments of the microfluidic chip, including redox mixing and the opening time of the stop-valve embedded into the side redox channel. The total turn-around time can be tuned according to the optimal interaction time of the antibody and antigen of interest. The Nyquist plots associated with the on-chip GFAP sensing for 10 to 10,000 pg mL^{-1} GFAP protein spiked in PBS are shown in Figure 3B. The results of the corresponding calibration curve show that the microfluidic-integrated GFAP immuno-biosensor assay detects GFAP within the linear detection range from 10 to 1000 pg mL^{-1}, with an LoD of 3.4 pg mL^{-1}, LoQ of 4.3 pg mL^{-1}, and sensitivity of 357.8 Ω mL pg^{-1} mm^{-2}. This detection range falls within the clinical detection range of GFAP in the blood of mTBI,[68] brain stroke,[69] and spinal cord injury[46] patients.

Moreover, 50, 100, and 500 pg mL^{-1} of GFAP protein were spiked in the human serum to assess its utility in PoC GFAP detection in clinical samples (Table S2). The GFAP-spiked serum samples were injected into the microfluidic chips. For the spiked serum samples containing 100 pg mL^{-1} of GFAP protein, ΔR_{ct} = 14.82 ± 0.70 kΩ, which is only 2.55 kΩ different from the signal for the sample concentration of GFAP spiked in PBS (ΔR_{ct} = 17.40 ± 0.15 kΩ). A similar response was detected for other concentrations of GFAP spiked in PBS and the serum. With the proximity between the calibration curves of PBS-spiked and serum-spiked samples (Figure 3C), it is concluded that there is no cross-reactivity or interference of the biosensor with serum components. The results confirm that the bio-ready electrodes are specifically beneficial for the development of automated bioassays since their simple fabrication and single-layer surface structure contribute to reliable signal generation under non-conventional on-chip sensing conditions. The microfluidic-integrated GFAP immuno-biosensor is useful as a PoC tool along with a portable potentiostat readout customized with the EIS module for rapid and on-site CNS injury detection (Figure S13).

4. CONCLUSIONS

In this study, a new fabrication approach was undertaken for the development of a novel self-contained conductive screen-printing ink. The ink contains PEDOT:PSS conductive polymers, with engineered chemistry for embedding the desired carboxyl functional groups into the graphene nanosheets, specifically applicable for electrochemical immunosensing. The electrodes printed using this new ink provide advantageous features over the conventional SPEs, by reducing the required surface modification down to just one antibody immobilization step, without the need for prior surface functionalization or enhancement. This fabrication approach, as a result, increases the overall reproducibility and scalability of electrochemical biosensors. The GFAP immuno-biosensor offered a wide detection range from 1 pg mL^{-1} to 10 ng mL^{-1}. The GiPEC electrodes also provided a desired antifouling feature, which is needed for detecting molecules of the target in complex clinical biofluids like the serum. The electrochemical characterization of GiPEC was compared against the commercially available SPEs and demonstrated their competitive biosensing properties at a lower manufacturing cost. Upon engineering and optimizing the composition of the inks, printing parameters, sensor preparation as well as microfluidic-based automating of the electrochemical biosensing assay, the self-contained biosensor exhibited a clinically relevant linear detection range, detection limit, and reproducibility in measuring GFAP in spiked PBS and human serum samples. Owing to the importance of rapid, accurate, and PoC detection of CNS diseases, the performance of the microfluidic-integrated biosensor exhibits its capability for PoC applications, for example, it can be useful for patients in the field or in remote settings where no trained personnel or access to expensive diagnostic facilities is available.

■ ASSOCIATED CONTENT

Supporting Information

The Supporting Information is available free of charge at https://pubs.acs.org/doi/10.1021/acsami.2c07322.

https://doi.org/10.1021/acsami.2c07322
ACS Appl. Mater. Interfaces 2022, 14, 28651−28662

Printing ink texture and designs of the strips, all steps of the strip fabrication, electrical resistivity equations and data, FESEM image of the antibody-coated electrodes, complementary AFM histograms, complementary EIS and CV characterization of the strips, reproducibility tests of commercialized DS-110 SPEs, and their comparison with GiPEC, electrochemical reaction mechanism tests, biofouling assessment, antibody/antigen incubation time optimization, complementary information on the design of the multi-layered microfluidic platform, data on the on-chip GFAP-spiked serum sample detection, and schematic illustration of the ultimate PoC portable system (PDF)

AUTHOR INFORMATION

Corresponding Author

Amir Sanati Nezhad − *BioMEMS and Bioinspired Microfluidic Laboratory, Department of Biomedical Engineering, Department of Mechanical and Manufacturing Engineering, and Biomedical Engineering Graduate Program, University of Calgary, Calgary, Alberta T2N 1N4, Canada;* orcid.org/0000-0002-2309-2388; Email: amir.sanatinezhad@ucalgary.ca

Authors

Razieh Salahandish − *BioMEMS and Bioinspired Microfluidic Laboratory, Department of Biomedical Engineering and Department of Mechanical and Manufacturing Engineering, University of Calgary, Calgary, Alberta T2N 1N4, Canada*

Fatemeh Haghayegh − *Department of Mechanical and Manufacturing Engineering, University of Calgary, Calgary, Alberta T2N 1N4, Canada*

Sultan Khetani − *Department of Mechanical and Manufacturing Engineering and Biomedical Engineering Graduate Program, University of Calgary, Calgary, Alberta T2N 1N4, Canada*

Mohsen Hassani − *Department of Mechanical and Manufacturing Engineering, University of Calgary, Calgary, Alberta T2N 1N4, Canada*

Complete contact information is available at: https://pubs.acs.org/10.1021/acsami.2c07322

Author Contributions

R.S. and F.H. contributed equally to this work. Concept and design: R.S.; Experimentation and Data acquisition: R.S., F.H., and S.K.; Data analysis and interpretation: R.S., F.H., M.H., and A.S.N.; Serum sample analysis: R.S. and F.H.; Drafting and revising the manuscript: R.S., F.H., S.K., M.H., and A.S.N.

Notes

The authors declare no competing financial interest.

ACKNOWLEDGMENTS

The authors acknowledge the Canadian Institutes of Health Research (CIHR) and Natural Sciences and Engineering Research of Canada (NSERC). The authors also acknowledge the Canada Research Chair, University of Calgary, and CMC—Microsystems, Canada, for supporting this research.

REFERENCES

(1) Gauglitz, G. Point-of-care platforms. *Annu. Rev. Anal. Chem.* **2014**, *7*, 297−315.

(2) Anik, Ü. Electrochemical medical biosensors for POC applications. *Medical Biosensors for Point of Care (POC) Applications*; Elsevier, 2017; pp 275−292.

(3) Salahandish, R.; Zargartalebi, H.; Janmaleki, M.; Khetani, S.; Azarmanesh, M.; Ashani, M. M.; Aburashed, R.; Vatani, M.; Ghaffarinejad, A.; Sanati-Nezhad, A. Reproducible and Scalable Generation of Multilayer Nanocomposite Constructs for Ultrasensitive Nanobiosensing. *Adv. Mater. Technol.* **2019**, *4*, 1900478.

(4) Mohammadi, M.; Zargartalebi, H.; Salahandish, R.; Aburashed, R.; Wey Yong, K.; Sanati-Nezhad, A. Emerging technologies and commercial products in exosome-based cancer diagnosis and prognosis. *Biosens. Bioelectron.* **2021**, *183*, 113176.

(5) Li, P.; Lee, G.-H.; Kim, S. Y.; Kwon, S. Y.; Kim, H.-R.; Park, S. From diagnosis to treatment: recent advances in patient-friendly biosensors and implantable devices. *ACS Nano* **2021**, *15*, 1960−2004.

(6) Farzin, L.; Shamsipur, M. Recent advances in design of electrochemical affinity biosensors for low level detection of cancer protein biomarkers using nanomaterial-assisted signal enhancement strategies. *J. Pharm. Biomed. Anal.* **2018**, *147*, 185−210.

(7) Shamsuddin, S. H.; Gibson, T. D.; Tomlinson, D. C.; McPherson, M. J.; Jayne, D. G.; Millner, P. A. Reagentless Affimer- and antibody-based impedimetric biosensors for CEA-detection using a novel non-conducting polymer. *Biosens. Bioelectron.* **2021**, *178*, 113013.

(8) Gogola, J. L.; Martins, G.; Gevaerd, A.; Blanes, L.; Cardoso, J.; Marchini, F. K.; Banks, C. E.; Bergamini, M. F.; Marcolino-Junior, L. H. Label-free Aptasensor for p24-HIV protein detection based on Graphene Quantum Dots as an electrochemical signal amplifier. *Anal. Chim. Acta* **2021**, *1166*, 338548.

(9) Zhao, Y.; Wang, B.; Hojaiji, H.; Wang, Z.; Lin, S.; Yeung, C.; Lin, H.; Nguyen, P.; Chiu, K.; Salahi, K.; Cheng, X.; Tan, J.; Cerrillos, B. A.; Emaminejad, S. A wearable freestanding electrochemical sensing system. *Sci. Adv.* **2020**, *6*, No. eaaz0007.

(10) Prabakaran, K.; Jandas, P. J.; Luo, J.; Fu, C.; Wei, Q. Molecularly imprinted poly (methacrylic acid) based QCM biosensor for selective determination of L-tryptophan. *Colloids Surf., A* **2021**, *611*, 125859.

(11) Haghayegh, F.; Salahandish, R.; Hassani, M.; Sanati-Nezhad, A. Highly Stable Buffer-Based Zinc Oxide/Reduced Graphene Oxide Nanosurface Chemistry for Rapid Immunosensing of SARS-CoV-2 Antigens. *ACS Appl. Mater. Interfaces* **2022**, *14*, 10844−10855.

(12) Salahandish, R.; Ghaffarinejad, A.; Omidinia, E.; Zargartalebi, H.; Majidzadeh-A, K.; Naghib, S. M.; Sanati-Nezhad, A. Label-free ultrasensitive detection of breast cancer miRNA-21 biomarker employing electrochemical nano-genosensor based on sandwiched AgNPs in PANI and N-doped graphene. *Biosens. Bioelectron.* **2018**, *120*, 129−136.

(13) Salahandish, R.; Ghaffarinejad, A.; Naghib, S. M.; Majidzadeh-A, K.; Sanati-Nezhad, A. A novel graphene-grafted gold nanoparticles composite for highly sensitive electrochemical biosensing. *IEEE Sens. J.* **2018**, *18*, 2513−2519.

(14) Sabahi, A.; Salahandish, R.; Ghaffarinejad, A.; Omidinia, E. Electrochemical nano-genosensor for highly sensitive detection of miR-21 biomarker based on SWCNT-grafted dendritic Au nanostructure for early detection of prostate cancer. *Talanta* **2020**, *209*, 120595.

(15) Salahandish, R.; Ghaffarinejad, A.; Naghib, S. M.; Niyazi, A.; Majidzadeh-A, K.; Janmaleki, M.; Sanati-Nezhad, A. Sandwich-structured nanoparticles-grafted functionalized graphene based 3D nanocomposites for high-performance biosensors to detect ascorbic acid biomolecule. *Sci. Rep.* **2019**, *9*, 1226−11.

(16) Pu, Z.; Zhang, X.; Yu, H.; Tu, J.; Chen, H.; Liu, Y.; Su, X.; Wang, R.; Zhang, L.; Li, D. A thermal activated and differential self-calibrated flexible epidermal biomicrofluidic device for wearable accurate blood glucose monitoring. *Sci. Adv.* **2021**, *7*, No. eabd0199.

(17) Cheng, Y.; Zheng, F.; Lu, J.; Shang, L.; Xie, Z.; Zhao, Y.; Chen, Y.; Gu, Z. Bioinspired multicompartmental microfibers from microfluidics. *Adv. Mater.* **2014**, *26*, 5184−5190.

(18) Cheng, Y.; Zhang, X.; Cao, Y.; Tian, C.; Li, Y.; Wang, M.; Zhao, Y.; Zhao, G. Centrifugal microfluidics for ultra-rapid fabrication of versatile hydrogel microcarriers. *Appl. Mater. Today* **2018**, *13*, 116−125.
(19) Jalali, M.; AbdelFatah, T.; Mahshid, S. S.; Labib, M.; Sudalaiyadum Perumal, A.; Mahshid, S. A hierarchical 3D nano-structured microfluidic device for sensitive detection of pathogenic bacteria. *Small* **2018**, *14*, 1801893.
(20) Barman, S. C.; Zahed, M. A.; Sharifuzzaman, M.; Ko, S. G.; Yoon, H.; Nah, J. S.; Xuan, X.; Park, J. Y. A Polyallylamine Anchored Amine-Rich Laser-Ablated Graphene Platform for Facile and Highly Selective Electrochemical IgG Biomarker Detection. *Adv. Funct. Mater.* **2020**, *30*, 1907297.
(21) Guler, Z.; Sarac, A. Electrochemical impedance and spectroscopy study of the EDC/NHS activation of the carboxyl groups on poly (ε-caprolactone)/poly (m-anthranilic acid) nanofibers. *Express Polym. Lett.* **2016**, *10*, 96.
(22) Ferguson, B. S.; Hoggarth, D. A.; Maliniak, D.; Ploense, K.; White, R. J.; Woodward, N.; Hsieh, K.; Bonham, A. J.; Eisenstein, M.; Kippin, T. E. Real-time, aptamer-based tracking of circulating therapeutic agents in living animals. *Sci. Transl. Med.* **2013**, *5*, 213ra165.
(23) Zupančič, U.; Jolly, P.; Estrela, P.; Moschou, D.; Ingber, D. E. Graphene Enabled Low-Noise Surface Chemistry for Multiplexed Sepsis Biomarker Detection in Whole Blood. *Adv. Funct. Mater.* **2021**, *31*, 2010638.
(24) Wisitsoraat, A.; Mensing, J. P.; Karuwan, C.; Sriprachuabwong, C.; Jaruwongrungsee, K.; Phokharatkul, D.; Daniels, T. M.; Liewhiran, C.; Tuantranont, A. Printed organo-functionalized graphene for biosensing applications. *Biosens. Bioelectron.* **2017**, *87*, 7−17.
(25) Khetani, S.; Kollath, V. O.; Eastick, E.; Debert, C.; Sen, A.; Karan, K.; Sanati-Nezhad, A. Single-step functionalization of poly-catecholamine nanofilms for ultra-sensitive immunosensing of ubiquitin carboxyl terminal hydrolase-L1 (UCHL-1) in spinal cord injury. *Biosens. Bioelectron.* **2019**, *145*, 111715.
(26) Lei, Y.; Butler, D.; Lucking, M. C.; Zhang, F.; Xia, T.; Fujisawa, K.; Granzier-Nakajima, T.; Cruz-Silva, R.; Endo, M.; Terrones, H. Single-atom doping of MoS2 with manganese enables ultrasensitive detection of dopamine: Experimental and computational approach. *Sci. Adv.* **2020**, *6*, No. eabc4250.
(27) Vashist, S. K.; Schneider, E. M.; Lam, E.; Hrapovic, S.; Luong, J. H. One-step antibody immobilization-based rapid and highly-sensitive sandwich ELISA procedure for potential in vitro diagnostics. *Sci. Rep.* **2014**, *4*, 4407.
(28) Mazzaracchio, V.; Tomei, M. R.; Cacciotti, I.; Chiodoni, A.; Novara, C.; Castellino, M.; Scordo, G.; Amine, A.; Moscone, D.; Arduini, F. Inside the different types of carbon black as nanomodifiers for screen-printed electrodes. *Electrochim. Acta* **2019**, *317*, 673−683.
(29) Kiew, L.-V.; Chang, C.-Y.; Huang, S.-Y.; Wang, P.-W.; Heh, C.-H.; Liu, C.-T.; Cheng, C.-H.; Lu, Y.-X.; Chen, Y.-C.; Huang, Y.-X.; Chang, S.-Y.; Tsai, H.-Y.; Kung, Y.-A.; Huang, P.-N.; Hsu, M.-H.; Leo, B.-F.; Foo, Y.-Y.; Su, C.-H.; Hsu, K.-C.; Huang, P.-H.; Ng, C.-J.; Kamarulzaman, A.; Yuan, C.-J.; Shieh, D.-B.; Shih, S.-R.; Chung, L.-Y.; Chang, C.-C. Development of flexible electrochemical impedance spectroscopy-based biosensing platform for rapid screening of SARS-CoV-2 inhibitors. *Biosens. Bioelectron.* **2021**, *183*, 113213.
(30) Zavanelli, N.; Yeo, W.-H. Advances in screen printing of conductive nanomaterials for stretchable electronics. *ACS Omega* **2021**, *6*, 9344−9351.
(31) Hyun, W. J.; Lim, S.; Ahn, B. Y.; Lewis, J. A.; Frisbie, C. D.; Francis, L. F. Screen printing of highly loaded silver inks on plastic substrates using silicon stencils. *ACS Appl. Mater. Interfaces* **2015**, *7*, 12619−12624.
(32) He, P.; Cao, J.; Ding, H.; Liu, C.; Neilson, J.; Li, Z.; Kinloch, I. A.; Derby, B. Screen-printing of a highly conductive graphene ink for flexible printed electronics. *ACS Appl. Mater. Interfaces* **2019**, *11*, 32225−32234.
(33) Hu, D.; Zhu, W.; Peng, Y.; Shen, S.; Deng, Y. Flexible carbon nanotube-enriched silver electrode films with high electrical conductivity and reliability prepared by facile screen printing. *J. Mater. Sci. Technol.* **2017**, *33*, 1113−1119.
(34) Peng, S.; Yu, Y.; Wu, S.; Wang, C.-H. Conductive polymer nanocomposites for stretchable electronics: material selection, design, and applications. *ACS Appl. Mater. Interfaces* **2021**, *13*, 43831−43854.
(35) Kayser, L. V.; Lipomi, D. J. Stretchable conductive polymers and composites based on PEDOT and PEDOT: PSS. *Adv. Mater.* **2019**, *31*, 1806133.
(36) Fan, X.; Nie, W.; Tsai, H.; Wang, N.; Huang, H.; Cheng, Y.; Wen, R.; Ma, L.; Yan, F.; Xia, Y. PEDOT: PSS for flexible and stretchable electronics: modifications, strategies, and applications. *Adv. Sci.* **2019**, *6*, 1900813.
(37) Power, A. C.; Gorey, B.; Chandra, S.; Chapman, J. Carbon nanomaterials and their application to electrochemical sensors: a review. *Nanotechnol. Rev.* **2018**, *7*, 19−41.
(38) Htwe, Y. Z. N.; Mariatti, M. Printed Graphene and Hybrid Conductive Inks for Flexible, Stretchable, and Wearable Electronics: Progress, Opportunities, and Challenges. *J. Sci.: Adv. Mater. Devices* **2022**, *7*, 100435.
(39) Sriprachuabwong, C.; Karuwan, C.; Wisitsorrat, A.; Phokharatkul, D.; Lomas, T.; Sritongkham, P.; Tuantranont, A. Inkjet-printed graphene-PEDOT: PSS modified screen printed carbon electrode for biochemical sensing. *J. Mater. Chem.* **2012**, *22*, 5478−5485.
(40) Medhi, A.; Baruah, S.; Singh, J.; Betty, C. A.; Mohanta, D. Au nanoparticle modified GO/PEDOT-PSS based immunosensor probes for sensitive and selective detection of serum immunoglobulin g (IgG). *Appl. Surf. Sci.* **2022**, *575*, 151775.
(41) Yen, Y.-K.; Chao, C.-H.; Yeh, Y.-S. A graphene-PEDOT: PSS modified paper-based aptasensor for electrochemical impedance spectroscopy detection of tumor marker. *Sensors* **2020**, *20*, 1372.
(42) Huang, R.; He, L.; Xia, Y.; Xu, H.; Liu, C.; Xie, H.; Wang, S.; Peng, L.; Liu, Y.; Liu, Y.; He, N.; Li, Z. A sensitive aptasensor based on a hemin/G-Quadruplex-assisted signal amplification strategy for electrochemical detection of gastric cancer exosomes. *Small* **2019**, *15*, 1900735.
(43) North, S. H.; Shriver-Lake, L. C.; Taitt, C. R.; Ligler, F. S. Rapid analytical methods for on-site triage for traumatic brain injury. *Annu. Rev. Anal. Chem.* **2012**, *5*, 35−56.
(44) Shemilt, M.; Boutin, A.; Lauzier, F.; Zarychanski, R.; Moore, L.; McIntyre, L. A.; Nadeau, L.; Fergusson, D. A.; Mercier, E.; Archambault, P.; Lamontagne, F.; Perron, C.; Léger, C.; Turgeon, A. F. Prognostic value of glial fibrillary acidic protein in patients with moderate and severe traumatic brain injury: a systematic review and meta-analysis. *Crit. Care Med.* **2019**, *47*, e522−e529.
(45) Khetani, S.; Ozhukil Kollath, V.; Kundra, V.; Nguyen, M. D.; Debert, C.; Sen, A.; Karan, K.; Sanati-Nezhad, A. Polyethylenimine modified graphene-oxide electrochemical immunosensor for the detection of glial fibrillary acidic protein in central nervous system injury. *ACS Sens.* **2018**, *3*, 844−851.
(46) Ahadi, R.; Khodagholi, F.; Daneshi, A.; Vafaei, A.; Mafi, A. A.; Jorjani, M. Diagnostic value of serum levels of GFAP, pNF-H, and NSE compared with clinical findings in severity assessment of human traumatic spinal cord injury. *Spine* **2015**, *40*, E823−E830.
(47) Smits, F. M. Measurement of sheet resistivities with the four-point probe. *Bell Syst. Tech. J.* **1958**, *37*, 711−718.
(48) Chiu, W. W.; Travaš-Sejdić, J.; Cooney, R. P.; Bowmaker, G. A. Studies of dopant effects in poly (3, 4-ethylenedi-oxythiophene) using Raman spectroscopy. *J. Raman Spectrosc.* **2006**, *37*, 1354−1361.
(49) Johra, F. T.; Lee, J.-W.; Jung, W.-G. Facile and safe graphene preparation on solution based platform. *J. Ind. Eng. Chem.* **2014**, *20*, 2883−2887.
(50) Zhang, W.; Jia, B.; Furumai, H. Fabrication of graphene film composite electrochemical biosensor as a pre-screening algal toxin detection tool in the event of water contamination. *Sci. Rep.* **2018**, *8*, 10686.
(51) Chang, S. H.; Chiang, C.-H.; Kao, F.-S.; Tien, C.-L.; Wu, C.-G. Unraveling the enhanced electrical conductivity of PEDOT: PSS thin

films for ITO-free organic photovoltaics. *IEEE Photonics J.* **2014**, *6*, 1−7.
(52) Ohayon, D.; Pitsalidis, C.; Pappa, A.-M.; Hama, A.; Zhang, Y.; Gallais, L.; Owens, R. M. Laser Patterning of Self-Assembled Monolayers on PEDOT: PSS Films for Controlled Cell Adhesion. *Adv. Mater. Interfaces* **2017**, *4*, 1700191.
(53) Phongphut, A.; Sriprachuabwong, C.; Wisitsoraat, A.; Tuantranont, A.; Prichanont, S.; Sritongkham, P. A disposable amperometric biosensor based on inkjet-printed Au/PEDOT-PSS nanocomposite for triglyceride determination. *Sens. Actuators, B* **2013**, *178*, 501−507.
(54) Ku, M.; Kim, J.; Won, J.-E.; Kang, W.; Park, Y.-G.; Park, J.; Lee, J.-H.; Cheon, J.; Lee, H. H.; Park, J.-U. Smart, soft contact lens for wireless immunosensing of cortisol. *Sci. Adv.* **2020**, *6*, No. eabb2891.
(55) Shamsazar, A.; Asadi, A.; Seifzadeh, D.; Mahdavi, M. A novel and highly sensitive sandwich-type immunosensor for prostate-specific antigen detection based on MWCNTs-Fe3O4 nanocomposite. *Sens. Actuators, B* **2021**, *346*, 130459.
(56) Amini, N.; Shamsipur, M.; Naderi, K.; Maleki, A. Construction of a highly sensitive immunosensor based on antibody immunoglobulin G/3-(trimethoxysilyl) propylamine/graphene oxide for antigen-specific immunoglobulin G detection. *Microchem. J.* **2022**, *176*, 107218.
(57) Rodríguez, A.; Burgos-Flórez, F.; Posada, J. D.; Cervera, E.; Zucolotto, V.; Sanjuán, H.; Sanjuán, M.; Villalba, P. J. Electrochemical Immunosensor for the Quantification of S100B at Clinically Relevant Levels Using a Cysteamine Modified Surface. *Sensors* **2021**, *21*, 1929.
(58) Soares, R. R. A.; Hjort, R. G.; Pola, C. C.; Parate, K.; Reis, E. L.; Soares, N. F. F.; McLamore, E. S.; Claussen, J. C.; Gomes, C. L. Laser-induced Graphene electrochemical Immunosensors for rapid and label-free monitoring of Salmonella enterica in chicken broth. *ACS Sens.* **2020**, *5*, 1900−1911.
(59) Zhang, X.; Shen, Y.; Shen, G.; Zhang, C. Simple and Effective Approach to Prepare an Epoxy-Functionalized Polymer and Its Application for an Electrochemical Immunosensor. *ACS Omega* **2021**, *6*, 3637−3643.
(60) Gomes-Filho, S. L. R.; Dias, A. C. M. S.; Silva, M. M. S.; Silva, B. V. M.; Dutra, R. F. A carbon nanotube-based electrochemical immunosensor for cardiac troponin T. *Microchem. J.* **2013**, *109*, 10−15.
(61) Tuteja, S. K.; Kukkar, M.; Suri, C. R.; Paul, A. K.; Deep, A. One step in-situ synthesis of amine functionalized graphene for immunosensing of cardiac marker cTnI. *Biosens. Bioelectron.* **2015**, *66*, 129−135.
(62) Wu, L.; Sha, Y.; Li, W.; Wang, S.; Guo, Z.; Zhou, J.; Su, X.; Jiang, X. One-step preparation of disposable multi-functionalized g-C3N4 based electrochemiluminescence immunosensor for the detection of CA125. *Sens. Actuators, B* **2016**, *226*, 62−68.
(63) Chen, H.; Zhang, B.; Cui, Y.; Liu, B.; Chen, G.; Tang, D. One-step electrochemical immunoassay of biomarker based on nanogold-functionalized graphene sensing platform. *Anal. Methods* **2011**, *3*, 1615−1621.
(64) Eissa, S.; Alshehri, N.; Rahman, A. M. A.; Dasouki, M.; Abu-Salah, K. M.; Zourob, M. Electrochemical immunosensors for the detection of survival motor neuron (SMN) protein using different carbon nanomaterials-modified electrodes. *Biosens. Bioelectron.* **2018**, *101*, 282−289.
(65) Zhang, X.; Shen, G.; Sun, S.; Shen, Y.; Zhang, C.; Xiao, A. Direct immobilization of antibodies on dialdehyde cellulose film for convenient construction of an electrochemical immunosensor. *Sens. Actuators, B* **2014**, *200*, 304−309.
(66) Welch, R. D.; Ayaz, S. I.; Lewis, L. M.; Unden, J.; Chen, J. Y.; Mika, V. H.; Saville, B.; Tyndall, J. A.; Nash, M.; Buki, A.; Barzo, P.; Hack, D.; Tortella, F. C.; Schmid, K.; Hayes, R. L.; Vossough, A.; Sweriduk, S. T.; Bazarian, J. J. Ability of serum glial fibrillary acidic protein, ubiquitin C-terminal hydrolase-L1, and S100B to differentiate normal and abnormal head computed tomography findings in patients with suspected mild or moderate traumatic brain injury. *J. Neurotrauma* **2016**, *33*, 203−214.
(67) Salahandish, R.; Ghaffarinejad, A.; Naghib, S. M.; Majidzadeh-A, K.; Zargartalebi, H.; Sanati-Nezhad, A. Nano-biosensor for highly sensitive detection of HER2 positive breast cancer. *Biosens. Bioelectron.* **2018**, *117*, 104−111.
(68) Vos, P. E.; Jacobs, B.; Andriessen, T. M. J. C.; Lamers, K. J. B.; Borm, G. F.; Beems, T.; Edwards, M.; Rosmalen, C. F.; Vissers, J. L. M. GFAP and S100B are biomarkers of traumatic brain injury: an observational cohort study. *Neurology* **2010**, *75*, 1786−1793.
(69) Ren, C.; Kobeissy, F.; Alawieh, A.; Li, N.; Li, N.; Zibara, K.; Zoltewicz, S.; Guingab-Cagmat, J.; Larner, S. F.; Ding, Y. Assessment of serum UCH-L1 and GFAP in acute stroke patients. *Sci. Rep.* **2016**, *6*, 24588.

https://doi.org/10.1021/acsami.2c07322
ACS Appl. Mater. Interfaces 2022, 14, 28651−28662